Functional connectivity in the resting brain: A network analysis of the default mode hypothesis

Michael D. Greicius*†‡, Ben Krasnow*, Allan L. Reiss*§¶, and Vinod Menon*§¶

Departments of *Psychiatry and Behavioral Sciences and †Neurology and Neurological Sciences, §Program in Neurosciences, and ¶Stanford Brain Research Center, Stanford University School of Medicine, Stanford, CA 94305-5719

Edited by Marcus E. Raichle, Washington University School of Medicine, St. Louis, MO, and approved November 12, 2002 (received for review August 21, 2002)

Functional imaging studies have shown that certain brain regions, including posterior cingulate cortex (PCC) and ventral anterior cingulate cortex (vACC), consistently show greater activity during resting states than during cognitive tasks. This finding led to the hypothesis that these regions constitute a network supporting a default mode of brain function. In this study, we investigate three questions pertaining to this hypothesis: Does such a resting-state network exist in the human brain? Is it modulated during simple sensory processing? How is it modulated during cognitive processing? To address these questions, we defined PCC and vACC regions that showed decreased activity during a cognitive (working memory) task, then examined their functional connectivity during rest. PCC was strongly coupled with vACC and several other brain regions implicated in the default mode network. Next, we examined the functional connectivity of PCC and vACC during a visual processing task and show that the resultant connectivity maps are virtually identical to those obtained during rest. Last, we defined three lateral prefrontal regions showing increased activity during the cognitive task and examined their resting-state connectivity. We report significant inverse correlations among all three lateral prefrontal regions and PCC, suggesting a mechanism for attenuation of default mode network activity during cognitive processing. This study constitutes, to our knowledge, the first resting-state connectivity analysis of the default mode and provides the most compelling evidence to date for the existence of a cohesive default mode network. Our findings also provide insight into how this network is modulated by task demands and what functions it might subserve.

Functional brain imaging has been widely used to study the neural basis of perception, cognition, and emotion. Such studies have traditionally focused on brain regions showing task-related increases in neural activity, i.e., greater activity during an experimental task than during a baseline state, typically rest or a sensory-motor control task with reduced cognitive demand. Recently, however, increasing attention has been focused on brain regions in which neural activity is greater during the baseline state than during an experimental task. Interest in this phenomenon, sometimes referred to as "deactivation," has been sparked by the finding that particular brain regions, including two midline regions, the posterior cingulate cortex (PCC) and ventral anterior cingulate cortex (vACC), consistently demonstrate such task-related decreases in activity across a broad range of cognitive tasks (1, 2). Using quantitative positron emission tomography, Raichle *et al.* (3) determined that these brain regions are in their baseline state when subjects rest with their eyes closed. They hypothesized that this set of brain regions constitutes an organized network, whose activity is ongoing during rest and suspended during performance of externally cued tasks, that supports a "default mode of brain function."

At present, however, it is not known whether brain regions that show task-related decreases in activity, such as the PCC and vACC, constitute tightly linked nodes in a single, tonically active resting-state network. The default mode hypothesis is based on the finding of relative decreases in neural activity during task performance compared with a baseline state. Direct evidence for temporal coherence of resting-state neural activity between regions in this hypothetical network is lacking. Detection of temporal coherence in such a network would (*i*) provide more compelling evidence for the existence of a default mode network, and (*ii*) enhance our understanding of neural activity in baseline states, thereby refining interpretations of "activation" and "deactivation" in functional imaging studies (4). More broadly, mapping such a network may provide insight into the neural underpinnings of a critical but poorly understood component of human consciousness variably referred to as "a conscious resting state" (2, 5), "stimulus-independent thought" (6), or a default mode of brain function (3).

A number of key questions remain, however, chief among them being whether the postulated network exists in the resting brain. If so, which brain regions are linked in the network, and what inferences can be made about the mental processes subserved by these regions? Is the network altered or disrupted during simple sensory processing tasks? How is the network modulated during performance of externally cued cognitive tasks?

To address these questions, we formulated the following hypotheses: (*i*) If the default mode network exists, then analyzing the resting-state connectivity of one of its key components should generate a (partial) map of the larger network. (*ii*) If the network is minimally disrupted during passive sensory processing tasks, then the connectivity maps generated during rest should be replicable in a passive visual processing task. (*iii*) If the network activity is suspended during performance of cognitively demanding externally cued tasks, then resting-state activity in the network may be inversely correlated with activity in brain regions that show task-related activations.

To test these hypotheses, we used functional MRI (fMRI) to examine brain activity in a group of 14 subjects under three different conditions: performance of a cognitive (working memory) task; passive viewing of a visual stimulus; and resting state with eyes closed. The working memory task was used to define regions in the PCC and vACC that showed task-related decreases in activity and regions in the lateral prefrontal cortex that showed task-related increases in activity. We then applied a functional connectivity MRI (fcMRI) analysis to the resting-state and visual processing data. Unlike fMRI analyses, fcMRI

This paper was submitted directly (Track II) to the PNAS office.

Abbreviations: ROI, region of interest; PCC, posterior cingulate cortex; vACC, ventral anterior cingulate cortex; fcMRI, functional connectivity MRI; VLPFC, ventrolateral prefrontal cortex; DLPFC, dorsolateral prefrontal cortex; IPC, inferior parietal cortex; ITC, inferolateral temporal cortex; MPFC, medial prefrontal cortex; OFC, orbitofrontal cortex; PHG, parahippocampal gyrus.

‡To whom correspondence should be addressed. E-mail: greicius@stanford.edu.

does not rely on a comparison of experimental and baseline conditions; rather, it detects interregional temporal correlations of blood oxygen level-dependent (BOLD) signal fluctuations. Regions whose BOLD signal fluctuations show a high degree of temporal correlation are presumed to constitute a tightly coupled neural network. To date, most fcMRI studies have explored primary motor and sensory networks (7–9). Recently, fcMRI has been successfully applied in examining interactions between brain regions involved in language (10). In this study, we determined the connectivity patterns of the PCC and the vACC during the resting state and the visual processing task. We also examined correlations in resting-state activity between the "activated" lateral prefrontal regions and regions implicated in the default mode network.

Methods

Subjects and Tasks. Fourteen healthy right-handed subjects (seven females) participated in this study after giving informed consent in accordance with Stanford University's Institutional Review Board. Their ages ranged from 18 to 25 years, with a mean age of 21.2 years.

All subjects underwent a resting-state scan first, followed by three tasks: a visuospatial working memory task, a visual processing task, and a face-processing task, all implemented in a standard block design. The order of these three tasks was counterbalanced across subjects. The face-processing task was not analyzed for this study and will not be described further.

Resting State. For the resting-state scan, subjects were instructed simply to keep their eyes closed and to not think of anything in particular. The scan lasted for 4 min.

Working Memory. The working memory task consisted of six alternating experimental and control epochs. Each experimental and control epoch consisted of 16 stimuli presented for 500 ms each, with a 1,500-ms interstimulus interval. The stimulus was the letter "O" presented in one of nine distinct spatial locations in a 3×3 matrix. In the experimental epoch, subjects were instructed to respond if the stimulus was in the same location, as it was two trials back. In the control epoch, the subject was instructed to respond if the stimulus was in the center position. Each epoch was preceded by a 4-s instruction regarding the specific task the subject should perform. In addition to these epochs, three rest epochs were placed at the beginning, middle, and end of the experiment. Total length of the task was 7 min 12 s. Further details are described elsewhere (11).

Visual Processing. The visual processing task consisted of experimental and control epochs that alternated every 20 s for 6 cycles. The control epoch consisted of a static black-and-white radial checkerboard pattern. In the experimental condition, the same pattern was inverted (white sections become black, and black sections become white) at a frequency of 8 Hz. In both the control and experimental conditions, subjects were instructed to passively view the checkerboard. Total length of the task was 4 min.

Imaging Methods. Functional images were acquired on a 3-T General Electric Signa scanner by using a standard General Electric whole-head coil. The scanner runs on an LX platform, with gradients in "MiniCRM" configuration (35 mT/m, SR 190 mT per m/s) and has a Magnex (Concord, CA) 3-T 80-cm magnet. The following spiral pulse sequence parameters were used: repeat time, 2,000 ms; echo time, 30 ms; flip angle, 80°; and 1 interleave. Twenty-eight axial slices (4-mm thick, 0.5-mm skip) parallel to the anterior commisure–posterior commisure line were acquired. To reduce blurring and signal loss arising from field inhomogeneities, an automated high-order shimming method based on spiral acquisitions was used before acquiring functional MRI data (12). To aid in the localization of functional data, a high-resolution T1-weighted spoiled grass gradient recalled 3D MRI sequence with the following parameters was used: 124 coronal slices, 1.5 mm thickness; no skip; repeat time, 11 ms; echo time, 2 ms; and flip angle, 15°. The images were reconstructed as a $124 \times 256 \times 256$ matrix with a $1.5 \times 0.9 \times 0.9$ mm spatial resolution. The structural scans were acquired on a 1.5-T General Electric Signa scanner.

Data Analysis. Data were preprocessed and analyzed by using SPM99 (www.fil.ion.ucl.ac.uk/spm). Images were corrected for movement by using least-square minimization without higher-order corrections for spin history and normalized (13) to stereotaxic coordinates of Talairach and Tournoux (14). Images were then resampled every 2 mm by using sinc interpolation and smoothed with a 4-mm Gaussian kernel to decrease spatial noise. Statistical analysis was performed on individual and group data by using the general linear model and Gaussian random fields theory as implemented in SPM99 (15). Group analyses were performed by using a random-effects model that estimates the error variance for each condition of interest across subjects, rather than across scans (16), and therefore provides a stronger generalization to the population from which data are acquired. Statistical maps were superimposed on normalized high-resolution T1-weighted images and their locations interpreted by using known neuroanatomical landmarks.

Regions of Interest (ROIs). Data from the working memory task were used to identify precise ROIs in brain areas that showed task-related decreases and increases in activity. For this purpose, a three-step process was undertaken.

(*i*) First, a random-effects analysis (height and extent thresholds of $P < 0.001$) was used to determine which brain regions showed task-related decreases in activity and which showed task-related increases in activity. Consistent with prior studies (1, 2), the analysis revealed significant task-related decreases in the PCC, vACC, medial prefrontal cortex (MPFC), and left inferior parietal cortex (IPC). Among these four regions, the PCC (Talairach coordinates: [−12 −47 32] and vACC [6 39−4]) had the highest peak *z* scores and were selected on this basis as the precise ROIs for fcMRI analysis. From among the regions showing task-related increases, we chose three lateral prefrontal cortex regions that commonly show increased activity during working memory (17): left ventrolateral prefrontal cortex (VLPFC) [−32 29−6], right VLPFC [38 25−10], and right dorsolateral prefrontal cortex (DLPFC) [44 36 17]. (*ii*) Next, to make the five ROIs uniform in size and more anatomically precise, the initial ROIs ranged in size from 175 to 1,514 voxels, the final group ROIs were selected as the most significant cluster of 40–50 voxels surrounding the maxima noted above. (*iii*) Finally, subject-specific ROIs were obtained by selecting the largest significant cluster showing task-related decreases within the PCC and vACC group ROIs and the largest significant cluster showing task-related increases within the three prefrontal group ROIs. For these subject-specific ROIs, we used a reduced height threshold of $P < 0.01$ given the restricted search field within the group ROIs. One subject had no significant "deactivation" cluster within the group PCC ROI, so data were analyzed for 13/14 subjects' PCC and 14/14 subjects' vACC. Similarly, one subject had no significant "activation" cluster within the group left VLPFC ROI, so data were analyzed for 13/14 subjects' left VLPFC, 14/14 subjects' right VLPFC, and 14/14 subjects' right DLPFC ROIs.

fcMRI Analyses. To perform the fcMRI analyses, time series from the resting-state scan were extracted for the subject-specific ROIs in the PCC and vACC by averaging the time

series of all voxels in the ROI. Before averaging individual voxel data, scaling and filtering steps were performed across all brain voxels as follows. To minimize the effect of global drift, voxel intensities were scaled by dividing each time point's value by the mean value of the whole-brain image at that time point. After this, the scaled waveform of each brain voxel was filtered by using a bandpass filter ($\approx 0.0083/\text{sec} < f < \approx 0.15/\text{sec}$) to reduce the effect of low-frequency drift and high-frequency noise (8). The resulting time series, representing the average intensity (after scaling and filtering) of all voxels in the ROI, was then used as a covariate of interest in a whole-brain, linear regression, statistical parametric analysis. Contrast images corresponding to this regressor were determined individually for each subject and entered into a second-level random-effects analysis (height and extent thresholds of $P < 0.001$) to determine the brain areas that showed significant functional connectivity across subjects. We also performed an identical analysis on the visual processing data.

For the lateral prefrontal cortex ROIs that showed working memory-related increases in activity, we examined regions that were significantly inversely correlated with the ROI time series during the resting-state scan. Because we had an *a priori* hypothesis related to these effects, we used a less conservative statistical threshold of $P < 0.01$ (height) and $P < 0.05$ (extent) for this whole-brain analysis.

Results

Behavioral Data. All subjects performed both experimental and control epochs of the working memory task with a high level of accuracy. The percentage of correct responses during the experimental epochs ranged from 89.6 to 99.0 (mean = 95.6, SD = 3.0). The percentage of correct responses in the control epochs ranged from 96.9 to 100 (mean = 99.6, SD = 0.01). The average reaction times for the experimental epochs ranged from 443.6 to 915.1 ms (mean = 682.5 ms, SD = 141.5). The average reaction times for the control epochs ranged from 287.5 to 759.4 ms (mean = 500.1 ms, SD = 131.9). The percentage of correct responses was significantly higher ($P < 0.001$, two-tailed paired t test) and the reaction times significantly faster ($P < 0.001$) during the control epochs compared with the experimental epochs.

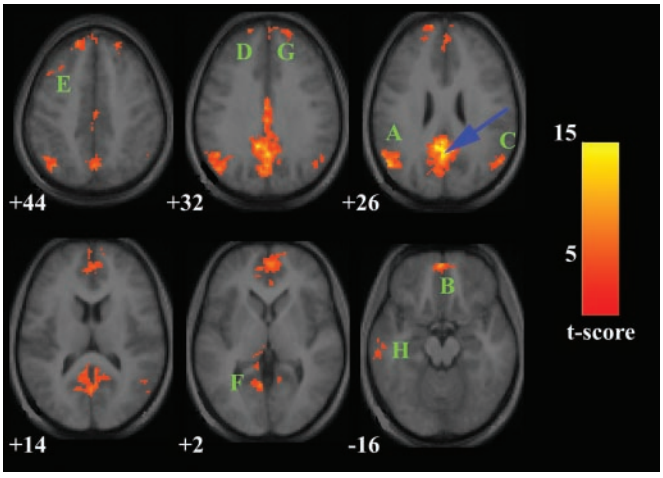

Fig. 1. Map of the resting-state neural connectivity for the PCC. The blue arrow indicates the approximate location of the PCC peak [−2 −51 27]. The approximate locations of the eight significant clusters are labeled A–H in descending order of the cluster's t score (A corresponds to the cluster with the highest t score). A [−51 −65 27], left IPC. B has a maximum at [−2 55 −18] in the OFC, but extends superiorly into the MPFC and the vACC (seen at $z = +2$). C [53 −61 27], right IPC. D [−16 49 38], MPFC just left of midline. E [−44 20 41], left DLPFC. F [−12 −35 0], posterior left PHG. G [18 54 32], MPFC just right of midline. H [−58 −18 −14], left ITC. Map is superimposed on transverse sections of the group-average structural scans. The numbers below each image refer to the z plane coordinates of Talairach and Tournoux. The left hemisphere of the brain corresponds to the left side of the image. Height and extent thresholds were set at $P < 0.001$. t score scale is shown on the right.

Table 1. Functional connectivity of the PCC during the resting state

Connected regions	BA	Cluster size, voxels	Maximal z-score primary peak	Primary peak location
PCC/precuneus	23/31/7	2937	6.39	−2, −51, 27
Left IPC	39/40	742	5.55	−51, −65, 27
OFC/MPFC/vACC	11/10/32	1376	5.38	−2, 55, −18
Right IPC	39/40	229	4.79	53, −61, 27
MPFC	8	365	4.71	−16, 49, 38
Left DLPFC	8/9	106	4.59	−44, 20, 41
Left PHG	30	92	4.44	−12, −35, 0
MPFC	9	141	4.32	18, 54, 32
Left ITC	20/21	126	4.05	−18, −14

Brain regions that showed significant connectivity to the PCC ROI centered at [2, −51, 27]. The height and extent thresholds were set at $P < 0.001$. BA, Brodmann's area.

Task-Related Decreases and Increases in Activity. ***Working memory.*** Task-related decreases were observed in the PCC and vACC, and task-related increases were observed in the lateral prefrontal ROIs as detailed in *Methods*. Further details regarding task-related decreases and increases in activity during the working memory task are published as Tables 3 and 4 in the supporting information on the PNAS web site, www.pnas.org. ***Visual processing.*** Task-related increases in activity were observed in extrastriate regions bilaterally when the flashing checkerboard epochs were contrasted with the static checkerboard epochs. No task-related decreases in activity were observed. Further details regarding task-related increases in activity are published as Table 5 in the supporting information on the PNAS web site.

Resting-State Connectivity Maps. ***PCC.*** The PCC showed significant resting-state connectivity with the following regions: a large cluster of MPFC, including vACC and orbitofrontal cortex

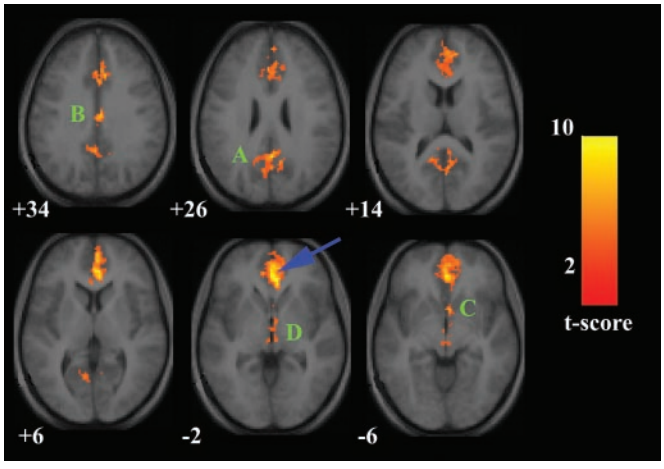

Fig. 2. Map of the resting-state neural connectivity for the vACC. The blue arrow indicates the approximate location of the vACC maximum [2 38 −2]. A [2 −51 27], PCC extending into the precuneus. B [4 −14 34], rostral PCC. C [4 9 −6], nucleus accumbens. D [4 −16 −3] is in the hypothalamus with some extension into the rostral midbrain. For other details, see Fig. 1.

Table 2. Functional connectivity of the vACC during the resting state

Connected regions	BA	Cluster size, voxels	Maximal *z*-score primary peak	Primary peak location
VACC/MPFC/OFC	32/10/11	2549	5.58	2, 38, −2
PCC/precuneus	23/31/7	813	5.05	2, −51, 27
Rostral PCC	23	243	4.82	4, −14, 34
Nucleus accumbens	N/A	112	4.52	4, 9, −6
Hypothalamus/midbrain	N/A	117	4.28	4, −16, −3

Brain regions that showed significant connectivity to the vACC ROI centered at [2, 38, −2]. The height and extent thresholds were set at $P < 0.001$. BA, Brodmann's area.

(OFC); left DLPFC; IPC bilaterally; left inferolateral temporal cortex (ITC); and left parahippocampal gyrus (PHG) (Fig. 1, Table 1).

vACC. The vACC showed significant resting-state connectivity with the following regions: PCC, MPFC/OFC, nucleus accumbens, and hypothalamus/midbrain (Fig. 2, Table 2).

Visual Processing Task Connectivity Maps. The connectivity patterns for the PCC and vACC during the visual processing task were virtually identical to those obtained from the resting-state data. Fig. 3 shows the connectivity patterns acquired for the PCC during the visual processing task compared with those acquired during the resting state. A similar figure (Fig. 5) comparing the vACC connectivity maps during the resting state and the visual processing task is published as supporting information on the PNAS web site. The precise locations for the cluster maxima for the PCC and vACC connectivity maps during the visual processing task are also published as Tables 6 and 7 in the supporting information on the PNAS web site.

Prefrontal Regions and Inverse Correlations. Fig. 4 shows the statistical maps for regions inversely correlated with the left VLPFC, right VLPFC, and right DLPFC during the resting state. In each case, only one cluster had resting-state activity that was significantly inversely correlated with the prefrontal ROI activity, and in each case the cluster was centered in the PCC.

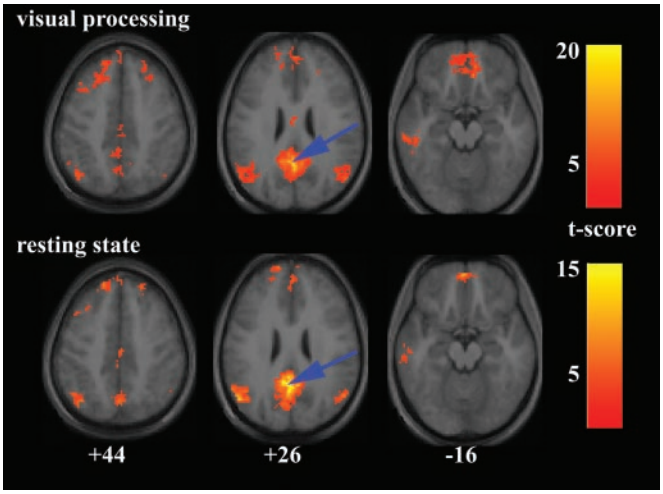

Fig. 3. Comparison of the PCC connectivity patterns during the visual processing task (*Upper*) and the resting-state (*Lower*). The blue arrows indicate the approximate location of the PCC peak [−2 −51 27]. For other details, see Fig. 1.

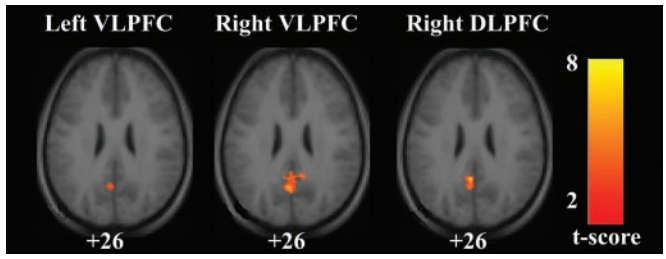

Fig. 4. Connectivity maps showing regions inversely correlated with the left VLPFC, the right VLPFC, and the right DLPFC. In each case, the only significant cluster was in the PCC. Maxima were at [−4 −55 25] for the left VLPFC, [0 −49 30] for the right VLPFC, and [−4 −49 26] for the right DLPFC. Height threshold was $P < 0.01$; extent threshold was $P < 0.05$. For other details, see Fig. 1.

Discussion

This is the first study, to our knowledge, to demonstrate resting-state functional connectivity between brain regions implicated in the default mode network (1, 3). The vACC showed significant functional connectivity with the PCC and the MPFC (Fig. 2), two regions implicated in the default mode network. The PCC connectivity map (Fig. 1), however, provided a far more complete match with the hypothesized default mode network. Of the eight regions cited by Shulman *et al.* (1) in their metaanalysis of positron emission tomography "deactivations," our PCC connectivity map includes all but the right amygdala and the left lateral inferior frontal cortex. Furthermore, only one of the regions (the left PHG) in the PCC connectivity map was not identified in the metaanalysis. This extensive overlap between our resting-state network analysis and the comparative approaches (baseline vs. experimental) combined in the meta-analysis suggests that the resting-state network identified here accounts, in large part, for the phenomenon of task-related decreases in brain activity. Taken together, our results demonstrate that a distinct set of brain regions, whose activity decreases during cognitive tasks compared with baseline states, shows significant functional connectivity during the resting state, thus providing the most compelling evidence to date for the existence of a cohesive, tonically active, default mode network.

Although the default mode network is thought to be most active during the resting state, it may also persist during passive sensory processing states (1, 2). To explore this possibility, we generated connectivity maps for the PCC and the vACC during our visual processing task and compared them to the resting-state maps. The PCC and vACC maps were virtually identical in the resting state and the visual processing task (Fig. 3 and supporting information on the PNAS web site), suggesting that the default mode neural network is minimally disrupted by sensory processing tasks with limited cognitive demand. It is important to note, in this regard, that the PCC and vACC were not "deactivated" in the visual processing task, further suggesting similar levels of ongoing activity in the default mode network during the flashing and still checkerboard epochs. This finding has important implications for the design and interpretation of functional imaging studies (4, 18). In particular, investigators wishing to study the functions subserved by regions such as the PCC or vACC should consider contrasting their experimental task with an equally demanding baseline task. Furthermore, because the default mode network was not significantly different between an eyes-closed and an eyes-open state, we may be able to deduce what cognitive processes the network does or does not support. For example, the default mode network appears to be distinct from the neural network that generates the alpha rhythm in resting electroencephalograms, given that the latter reproducibly attenuates when a subject opens their eyes (19).

Although the default mode network appears to persist during sensory tasks with low cognitive demand, it has been suggested that externally cued tasks with high cognitive demand do modulate the network, contributing to the phenomenon of task-related decreases in brain activity (4). If this network is suspended during performance of such tasks, we reasoned that during the resting state, the default mode network and brain regions that show task-related increases in brain activity may be inversely correlated. This hypothesis was strongly supported by the finding of significant inverse correlations between all three "activated" lateral prefrontal ROIs and the PCC during rest (Fig. 4). In this regard, it should be noted that Hampson *et al.* (10) also detected a negative correlation between activity in Broca's area and activity in the PCC during a passive listening task. These findings suggest the presence, during rest, of an inhibitory interaction between activated regions and regions in the default mode network, particularly the PCC. This raises the possibility that activated prefrontal regions, when called to duty, directly suppress the default mode network (20). Alternatively, it is possible that these regions are maintained in antagonistic states by a third region. The thalamus, for example, is one such subcortical region that has been shown to play an intermediary role in cortico–cortical interactions (21).

We will now consider the question of what mental processes the default mode network might subserve. Several findings from our study suggest that the PCC plays a central role in the default mode network. First, of the regions that showed task-related decreases during working memory and that also overlapped with regions in the default mode network (outlined by Raichle *et al*. in ref. 3), the PCC had the second highest *z* score. Second, compared with the vACC connectivity map, the PCC connectivity map provided a better match with this default mode network (accounting for six of eight regions cited in the initial metaanalysis) (1). Third, in the resting state, the PCC was the only region in the brain to show inverse correlations with any of the "activated" prefrontal ROIs. Finally, the PCC appeared not only in one of these inverse correlation maps, but in each of the three. The attribution of a central role to the PCC is consistent with data showing that the PCC is one of the most metabolically active regions during rest (3), that its activity decreases as a function of waning consciousness during sedation (22), and that its connections to prefrontal regions are impaired in the persistent vegetative state (23).

In view of these observations, understanding the cognitive functions of the PCC may yield insight into the functions supported by the default mode network. Unfortunately, imaging studies have revealed relatively little about the functions of the PCC, presumably because most paradigms have used a baseline state (such as fixation or sensory processing) in which the PCC is already active. Recently, however, a handful of imaging studies using more complex baseline states have implicated the PCC in retrieval of episodic memories (24–27). In this regard, the study by Cabeza *et al.* (27) is particularly instructive, in that the PCC did not show increased activity when an episodic memory retrieval task was compared with a baseline of visual fixation; however, the PCC did show increased activity when the retrieval task was compared with a more complex baseline. That the PCC may be critical to the retrieval of episodic memories is further supported by the fact that it is consistently among the earliest brain regions to show decreased metabolism in Alzheimer's disease (28, 29). Finally, axonal tracing studies (30, 31) have demonstrated neural connectivity between the PCC and medial temporal lobe regions, such as the entorhinal cortex and PHG, known to be key memory centers across species.

It would seem, therefore, that if the PCC is a critical node in the default mode network, this network should be integrally involved with episodic retrieval. Indeed, one prevailing view is that the default mode or "conscious resting state" involves retrieval and manipulation of past events, both personal and general, in an effort to solve problems and develop future plans (2, 5). In this framework, the left DLPFC is commonly implicated in working memory (32) as well as retrieval of episodic memories (33). Similarly, the bilateral IPC are frequently activated during working memory paradigms in both humans and animals (34, 35). The left ITC is known to be a major repository for semantic knowledge (36). The left PHG is associated with memory in humans (37), and its connections with the PCC may contribute to memory processes in animals (38). Perhaps the most substantial corroborative evidence to support our claim that the default mode network participates in retrieval of information, both personal and general, stems from the study by Maguire and Mummery (24). In that study, the authors compared a combination of four types of retrieval (personal memories, personal facts; nonpersonal memories, nonpersonal facts) with a relatively complex baseline (attending to syllable count while listening to words) and showed increased activity in a network that overlaps considerably with the default mode network outlined here. In particular, increased activity was detected in the PCC, the bilateral IPC, the MPFC, the left PHG, and the left ITC (*ibid*, Fig. 1).

Thus, the regions linked to the PCC in the default mode network are well-suited to support the mental processes presumed to be ongoing during the resting state. In contrast to the PCC and its connections to higher cortical regions, the vACC is linked primarily to paralimbic and subcortical regions associated with affective and autonomic processes including OFC, nucleus accumbens, and hypothalamus/midbrain (39, 40). The distinct roles demonstrated for PCC and vACC in our study converge on a model, derived from functional imaging studies of depression, positing that the vACC links a ventral "vegetative–somatic" compartment with a dorsal "attention–cognition" compartment that includes the PCC (41). Further support for this model is found in the overlap of the PCC and vACC patterns. The OFC and the MPFC, which have been implicated in the integration of cognitive and emotional stimuli (39, 42, 43) and also project to subcortical regions including nucleus accumbens and hypothalamus (44, 45), were the only regions common to both the PCC and vACC connectivity patterns. Thus, robust functional connections between PCC and vACC appear to form the critical link in the network between higher cortical (presumably conscious) processing and more basic (possibly subconscious) processing necessary for calibrating affective and autonomic states.

In summary, we have provided compelling evidence for the existence of a default mode network in the resting state. We have also shown that this network is minimally disrupted during a visual processing task and suggested that it is maintained in a dynamic equilibrium with lateral prefrontal regions that commonly show task-related increases in activity. Although the precise mental processes supported by the default mode network remain to be elucidated, we suggest that the retrieval and manipulation of episodic memories and semantic knowledge are likely candidates. A clearer understanding of the default mode network will be critical in the proper interpretation of task-activation studies that involve comparing an experimental task with a resting or simple-processing baseline. Understanding this network should also have broader implications. As interest builds in defining different components of consciousness and their neural correlates (46), several features of the default mode network, that it is widely distributed, internally cued, appears to integrate cognitive and emotional processing, and can be experimentally modulated, should make it an important and rewarding area of study in this nascent field.

This work was made possible through grants from the National Institutes of Health (MH19938, MH01142, HD31715, HD40761, and MH62430), the Ruth K. Broad Biomedical Research Foundation, and the Sinclair Fund.

1. Shulman, G. L., Fiez, J. A., Corbetta, M., Buckner, R. L., Miezin, F. M., Raichle, M. E. & Petersen, S. E. (1997) *J. Cognit. Neurosci.* **9,** 648–663.
2. Mazoyer, B., Zago, L., Mellet, E., Bricogne, S., Etard, O., Houde, O., Crivello, F., Joliot, M., Petit, L. & Tzourio-Mazoyer, N. (2001) *Brain Res. Bull.* **54,** 287–298.
3. Raichle, M. E., MacLeod, A. M., Snyder, A. Z., Powers, W. J., Gusnard, D. A. & Shulman, G. L. (2001) *Proc. Natl. Acad. Sci. USA* **98,** 676–682.
4. Gusnard, D. A. & Raichle, M. E. (2001) *Nat. Rev. Neurosci.* **2,** 685–694.
5. Binder, J. R., Frost, J. A., Hammeke, T. A., Bellgowan, P. S., Rao, S. M. & Cox, R. W. (1999) *J. Cognit. Neurosci.* **11,** 80–95.
6. McGuire, P. K., Paulesu, E., Frackowiak, R. S. & Frith, C. D. (1996) *NeuroReport* **7,** 2095–2099.
7. Biswal, B., Yetkin, F. Z., Haughton, V. M. & Hyde, J. S. (1995) *Magn. Reson. Med.* **34,** 537–541.
8. Lowe, M. J., Mock, B. J. & Sorenson, J. A. (1998) *NeuroImage* **7,** 119–132.
9. Cordes, D., Haughton, V. M., Arfanakis, K., Carew, J. D., Turski, P. A., Moritz, C. H., Quigley, M. A. & Meyerand, M. E. (2001) *Am. J. Neuroradiol.* **22,** 1326–1333.
10. Hampson, M., Peterson, B. S., Skudlarski, P., Gatenby, J. C. & Gore, J. C. (2002) *Hum. Brain Mapp.* **15,** 247–262.
11. Kwon, H., Reiss, A. L. & Menon, V. (2002) *Proc. Natl. Acad. Sci. USA* **99,** 13336–13341.
12. Kim, D., Adalsteinsson, E., Glover, G. & Spielman, S. (2000) in *Proceedings of the 8th Annual Meeting of ISMRM* (ISMRM, Denver), p. 1685.
13. Friston, K. J., Ashburner, J., Frith, C. D., Poline, J. B., Heather, J. D. & Frackowiak, R. S. D. (1995) *Hum. Brain Mapp.* **2,** 165–189.
14. Talairach, J. & Tournoux, P. (1988) *Co-Planar Stereotaxic Atlas of the Human Brain* (Thieme, New York).
15. Friston, K. J., Holmes, A. P., Worsley, K. J., Poline, J. B., Frith, C. D. & Frackowiak, R. S. J. (1995) *Hum. Brain Mapp.* **2,** 189–210.
16. Holmes, A. P. & Friston, K. J. (1998) *NeuroImage* **7,** S754.
17. Fletcher, P. C. & Henson, R. N. (2001) *Brain* **124,** 849–881.
18. Stark, C. E. & Squire, L. R. (2001) *Proc. Natl. Acad. Sci. USA* **98,** 12760–12766.
19. Binnie, C. D. & Prior, P. F. (1994) *J. Neurol. Neurosurg. Psychiatry* **57,** 1308–1319.
20. Knight, R. T., Staines, W. R., Swick, D. & Chao, L. L. (1999) *Acta Psychol. (Amsterdam)* **101,** 159–178.
21. Sherman, S. M. (2001) *Prog. Brain Res.* **134,** 51–69.
22. Fiset, P., Paus, T., Daloze, T., Plourde, G., Meuret, P., Bonhomme, V., Hajj-Ali, N., Backman, S. B. & Evans, A. C. (1999) *J. Neurosci.* **19,** 5506–5513.
23. Laureys, S., Goldman, S., Phillips, C., Van Bogaert, P., Aerts, J., Luxen, A., Franck, G. & Maquet, P. (1999) *NeuroImage* **9,** 377–382.
24. Maguire, E. A. & Mummery, C. J. (1999) *Hippocampus* **9,** 54–61.
25. Maddock, R. J., Garrett, A. S. & Buonocore, M. H. (2001) *Neuroscience* **104,** 667–676.
26. Fujii, T., Okuda, J., Tsukiura, T., Ohtake, H., Miura, R., Fukatsu, R., Suzuki, K., Kawashima, R., Itoh, M., Fukuda, H. & Yamadori, A. (2002) *NeuroImage* **15,** 501–508.
27. Cabeza, R., Dolcos, F., Graham, R. & Nyberg, L. (2002) *NeuroImage* **16,** 317–330.
28. Minoshima, S., Giordani, B., Berent, S., Frey, K. A., Foster, N. L. & Kuhl, D. E. (1997) *Ann. Neurol.* **42,** 85–94.
29. Johnson, K. A., Jones, K., Holman, B. L., Becker, J. A., Spiers, P. A., Satlin, A. & Albert, M. S. (1998) *Neurology* **50,** 1563–1571.
30. Suzuki, W. A. & Amaral, D. G. (1994) *J. Comp. Neurol.* **350,** 497–533.
31. Morris, R., Petrides, M. & Pandya, D. N. (1999) *Eur. J. Neurosci.* **11,** 2506–2518.
32. Petrides, M. (2000) *Exp. Brain Res.* **133,** 44–54.
33. Desgranges, B., Baron, J. C. & Eustache, F. (1998) *NeuroImage* **8,** 198–213.
34. Friedman, H. R. & Goldman-Rakic, P. S. (1994) *J. Neurosci.* **14,** 2775–2788.
35. Jonides, J., Schumacher, E. H., Smith, E. E., Koeppe, R. A., Awh, E., Reuter-Lorenz, P. A., Marshuetz, C. & Willis, C. R. (1998) *J. Neurosci.* **18,** 5026–5034.
36. Warburton, E., Wise, R. J., Price, C. J., Weiller, C., Hadar, U., Ramsay, S. & Frackowiak, R. S. (1996) *Brain* **119,** 159–179.
37. Saykin, A. J., Johnson, S. C., Flashman, L. A., McAllister, T. W., Sparling, M., Darcey, T. M., Moritz, C. H., Guerin, S. J., Weaver, J. & Mamourian, A. (1999) *Brain* **122,** 1963–1971.
38. Vogt, B. A., Finch, D. M. & Olson, C. R. (1992) *Cereb. Cortex* **2,** 435–443.
39. Damasio, A. R., Grabowski, T. J., Bechara, A., Damasio, H., Ponto, L. L., Parvizi, J. & Hichwa, R. D. (2000) *Nat. Neurosci.* **3,** 1049–1056.
40. Aharon, I., Etcoff, N., Ariely, D., Chabris, C. F., O'Connor, E. & Breiter, H. C. (2001) *Neuron* **32,** 537–551.
41. Mayberg, H. S. (1997) *J. Neuropsychiatry Clin. Neurosci.* **9,** 471–481.
42. Simpson, J. R., Jr., Snyder, A. Z., Gusnard, D. A. & Raichle, M. E. (2001) *Proc. Natl. Acad. Sci. USA* **98,** 683–687.
43. Simpson, J. R., Jr., Drevets, W. C., Snyder, A. Z., Gusnard, D. A. & Raichle, M. E. (2001) *Proc. Natl. Acad. Sci. USA* **98,** 688–693.
44. Ongur, D. & Price, J. L. (2000) *Cereb. Cortex* **10,** 206–219.
45. Barbas, H. (2000) *Brain Res. Bull.* **52,** 319–330.
46. Crick, F. & Koch, C. (1995) *Nature* **375,** 121–123.